Identifying Tibio-Femoral Joint Kinematics: Individual Adjustment versus Numerical Robustness ⋆

Irene Reichl * **Winfried Auzinger** **

* *University of Vienna, Centre for Sport Science and University Sports, Department for Biomechanics/Kinesiology and Applied Computer Science, AT-1150 Vienna, Austria (e-mail: Irene.Reichl@univie.ac.at).*
** *Vienna University of Technology, Institute for Analysis and Scientific Computing, AT-1040 Vienna, Austria.*

Abstract: The interpretation of joint kinematics data in terms of displacements is sensitive to the type of movement, the measurement technique and the reference axes where rotations and translations are associated with. Misaligned knee joint axes do not only lead to a misinterpretation of knee joint kinematics but, additionally, have a general impact on lower body kinematics. Therefore, several groups independently propose to *a posteriori* replace empirically palpated axes by functionally calculated axes. Flexion is the most dominant motion of the knee joint. Thus, the flexion axis has the largest effect on the kinematical calculation. The large angular flexion range facilitates the mathematical procedure of axis determination. The second rotation of importance is the internal/external rotation which is sometimes controlled by mathematical optimization techniques.

This contribution focuses on the evaluation of the concepts of *symmetrical axis of rotation approach* (SARA) and *finite helical axis* (FHA) regarding their applicability in axis reorientation procedures, and to explore which of the two underlying algorithms performs most robust and convenient under typical data perturbations.

Keywords: knee joint; joint displacement; accuracy; parameter optimization; axes calculation; FHA; discretization; SARA; SVD; singular value

1. INTRODUCTION

Diarthrodial joints can be kinematically described as an articulation between two rigid bodies, e.g., femur and tibia for the tibio-femoral joint (TFJ). Thus, general motion in 3D has six degrees of freedom (DOF), three DOF of rotation and three DOF of translation. The description of a six DOF displacement may involve the definition of three axes in order to associate rotation and translation with. This axis determination is highly susceptible to measurement errors or noise. Deviations in the defined axes have an important impact on the calculated displacements at the level of the knee joint and, in lower body optimizations, on the respective kinematics. Thus, it has to be ensured that the computed displacements are the most reproducible and comparable between different groups and clinics.

In this context, functional calculation of joint axes is convenient in order to reduce observer dependence of landmark based methods directly relating palpated marker positions to joint axes and centers. Nevertheless, also the mathematical calculation of rotational axes is influenced by marker placement, as any marker location involves a certain error induced by soft tissue artifacts (STA). Furthermore, a deviation of a marker at a smaller distance from the joint axis distorts the mathematical calculation more than the same deviation on a larger radius. Ehrig et al. (2011); Heller et al. (2011) define a measure for the quality of a marker position based on the residual of a minimized objective function.

Moreover, the validity of results obtained by parameter identification is a consequence of the degree of congruency between the function optimized and the kinematic mechanism of the joint in question. The most simple optimization approaches confine motion to rotation about a single cylinder hinge axis or a spherical joint center (Schwartz and Rozumalski (2005); Ehrig et al. (2006, 2007)). There exist more complex models as well, e.g., the compound hinge model (Churchill et al. (1998); Marin et al. (2003); Martelli et al. (2002)), where three axes are optimized. The algorithms perform best if the range of motion (ROM) of one body with respect to the other covers the physiologically largest possible angular range. Thus, in the experimental protocol, suitable movements are required ensuring the coverage of a wide range of the possible motion of the joint. For the hip joint center, Camomilla et al. (2006) propose the star arc movement. In clinical gait analysis, the ROM is limited due to pain or functional abnormities compromising the calculation.

Avoiding the definition of three axes for rotation and translation, the six DOF displacement may be described

⋆ This work was supported by the FWF Austrian Science Fund, contract number T318-N14.

as a (scalar) rotation and (scalar) translation about the same axis, i.e., the screw or the helical axis (Woltring et al. (1987)). The axis defined by observing a single instance of time is called the *instantaneous helical axis* (IHA), the averaged one is the *finite helical axis* (FHA).

The objective of this contribution is a quantitative comparison of the application of the screw axis concept and a simple cylindrical hinge axis, regarding the determination of the flexion axis and its integration in an axes reorientation procedure. The hinge axis is determined via the *Symmetrical Axis of Rotation Approach* (SARA, Ehrig et al. (2007)). The particular aspect of the influence of perturbed measurements is accounted for.

All computations were performed in MATLAB. [1]

List of abbreviations

`AoR` axis of rotation
`CoR` center of rotation
`DOF` degrees of freedom
`FE` **axis** flexion-extension axis
`FHA` finite helical axis
`ie` internal/external
`IHA` instantaneous helical axis
`JCS` joint coordinate system
`LCS` local coordinate system
`R` rotation
`ROM` range of motion
`SARA` symmetrical axis of rotation approach
`SCoRE` symmetrical center of rotation estimation
`STA` soft tissue artifacts
`T` translation
`TFJ` tibio-femoral joint
`TR` **axis** tibial-rotation axis
`GCS` global coordinate system
`LCS` local coordinate system
`SVD` singular value decomposition
`vv` varus/valgus

2. METHODS

2.1 Reference axes for joint displacements

The IHA is a powerful tool offering an invariant *six DOF (3R/3T)* description of an instantaneous displacement (Woltring et al. (1987)). The averaged IHA, i.e., the FHA, provides *two DOF (1R/1T)*. Also *two DOF*, namely *two rotational DOF*, are obtained in terms of the compound hinge model already mentioned in Section 1. The most simple axis has *one rotational DOF*, calculated e.g. by means of SARA which, in a least squares sense, fits a single hinge axis to preselected parts of the data set. Analogously to the IHA, we suggest that the instantaneous application of SARA yields a *three rotational DOF* description. Table 1 summarizes the number of rotational and translational DOF for the axes under consideration.

For clinical applications, none of these axes will in itself appropriately and comprehensively describe any given human joint. The IHA would be suitable; however, its practical computation requires a typically error-prone time discretization and its clinical interpretation is difficult. Therefore smart combinations of the mathematically calculated axes and a clinically meaningful description will be convenient. As an example, the compound hinge model mentioned in Section 1 was used to modify the post-processing of clinical kinematic analysis. In other terms, the clinically approved protocol is conserved but, preceding the calculation of joint displacements, the empirically palpated axes are replaced by mathematically calculated ones. Former implementations, e.g., Marin et al. (2003); Martelli et al. (2002), replace the anatomically defined flexion axis by the calculated FHA for a squat movement. The angular range of the mean FHA calculation is the flexion interval of $(40°, 80°)$ as therein the IHA is fairly stable. The remaining two axes are reoriented such that varus/valgus (vv) rotation is minimized. Then, the six DOF displacement is calculated by conventional algorithms.

In this study we adopt and extend the described axis reorientation approach. We compare the application of SARA and FHA for the reorientation of the anatomically defined flexion axis. The resulting rotations and translations are represented in the joint coordinate system (JCS) of Grood and Suntay (1983).

Table 1. DOF of different axis concepts.

DOF	type	rotation	translation
1	SARA: uniaxial	1	
2	FHA: uniaxial	1	1
	compound hinge joint	2	
3	instantaneous SARA	3	
6	IHA	3	3

2.2 Spherical center or cylindrical axis of rotation

Two body-fixed local coordinate systems (LCS) are defined corresponding to the two segments where CoR or AoR remain constant (Schwartz and Rozumalski (2005); Ehrig et al. (2006, 2007)). Rigid body transformations are defined, i.e., the rotations $R_j(t_i)$ of the segment coordinate system's principal axes and the translations $\boldsymbol{d}_j(t_i)$ of the segment coordinate system's origin. Indices $j = 1, 2$ refer to segment one and two, whereas t_i denotes the time step i, $i = 1 \dots N$. The matrices $R_j(t_i)$ and vectors $\boldsymbol{d}_j(t_i)$ relate an observed reference marker set (at a certain fixed time step) to the time varying marker configuration in the global laboratory coordinate system (GCS), see Fig. 2 in Ehrig et al. (2006).

Let $\boldsymbol{c}_j$ be the fixed CoR or a point on the AoR in the LCS j, respectively. Then the same point is given in the GCS by

$$\boldsymbol{c}_G(t_i) = R_j(t_i)\boldsymbol{c}_j + \boldsymbol{d}_j(t_i)\,, \quad j = 1, 2\,. \tag{1}$$

Schwartz and Rozumalski (2005) solve (1) at high numerical cost, calculating axes between any combination of time steps. Hereafter, nearest points between pairwise axes are computed. Finally, the CoR is defined as the median of all nearest points.

Alternatively, the *Symmetrical CoR Estimation* (SCoRE) (Ehrig et al. (2006)) or the SARA (Ehrig et al. (2007)) solve (1) by simultaneous minimization of the squared error in both LCSs, yielding the objective function (Eqn. 19 in Ehrig et al. (2006))

[1] MATLAB is a trademark of MathWorks, Inc.

$$f(\boldsymbol{c}_1, \boldsymbol{c}_2) = \sum_i \| \left(R_1(t_i)\boldsymbol{c}_1 - \boldsymbol{d}_1(t_i)\right) - \left(R_2(t_i)\boldsymbol{c}_2 - \boldsymbol{d}_2(t_i)\right) \|^2. \tag{2a}$$

This is equivalent to the linear least squares problem

$$\left\| \boldsymbol{R} \begin{pmatrix} \boldsymbol{c}_1 \\ \boldsymbol{c}_2 \end{pmatrix} - \boldsymbol{d} \right\|_2 \rightarrow \min, \tag{2b}$$

with

$$\boldsymbol{R} = \begin{pmatrix} R_1(t_1) & ; & -R_2(t_1) \\ \vdots & & \vdots \\ R_1(t_N) & ; & -R_2(t_N) \end{pmatrix}, \quad \boldsymbol{d} = \begin{pmatrix} \boldsymbol{d}_1(t_1) - \boldsymbol{d}_2(t_1) \\ \vdots \\ \boldsymbol{d}_1(t_N) - \boldsymbol{d}_1(t_N) \end{pmatrix}. \tag{2c}$$

Rank of the least squares problem (2): The rank r of the $(3N \times 6)$-matrix $\boldsymbol{R}$ in (2) determines the dimension of the solution space. If $\boldsymbol{R}$ has full rank, i.e., $r = 6$, this represents a spherical joint with a unique CoR. For given planar movement, however, the rank reduces by 1, yielding $r = 5$. In this case, there is a one-dimensional set of solutions $(\boldsymbol{c}_1, \boldsymbol{c}_2)$ representing an AoR fixed by position and direction. However, measurement error renders the matrix rank complete, thus, virtually implying a single point solution.

Computation of an AoR: For planar movement and zero noise, solution of (2) via the SVD, $\boldsymbol{R} = U\,\Sigma\,V^T$, delivers a particular vector

$$(\boldsymbol{c}_1, \boldsymbol{c}_2)^T = \boldsymbol{R}^+\boldsymbol{d} = V\,\Sigma^+ U^T\boldsymbol{d} \tag{3}$$

minimizing the objective function $f(\boldsymbol{c}_1, \boldsymbol{c}_2)$ from (2a) and with minimal norm in the six-dimensional coordinate system. This vector defines a reference point on the axis. The smallest singular value σ_6 vanishes. The corresponding singular vector $\boldsymbol{v}_6$ spans the one-dimensional null space of $\boldsymbol{R}$ and represents the direction of the axis in both LCS.

In the presence of noise, σ_6 will be finite but small and is to be interpreted as a perturbation measure. $\boldsymbol{v}_6$ can be interpreted as an approximate axis direction, and σ_6 measures the amount of movement of this approximate axis. Replacing σ_6 by zero is the natural way to deal with the effect of noise. This means that $\boldsymbol{R} = U\,\Sigma\,V^T$ is replaced by $\boldsymbol{R}_0 = U\,\Sigma_0 V^T$ with $\Sigma_0 = \mathrm{diag}(\sigma_1, \ldots, \sigma_5, 0)$ corresponding to nearby data representing planar movement. Again we obtain a minimal solution vector $(\boldsymbol{c}_1, \boldsymbol{c}_2)^T = \boldsymbol{R}_0^+\boldsymbol{d}$ representing a reference point on the axis.

The coordinates in the GCS are obtained by application of (1). As a consequence of measurement noise, the calculated CoR or AoR due to $\boldsymbol{c}_1$ and $\boldsymbol{c}_2$ in the LCSs do not necessarily coincide in the GCS. Following the suggestion of Ehrig et al. (2006), $\boldsymbol{c}$ is defined in the GCS as the mean between these two positions.

2.3 The instantaneous helical axis (IHA)

In the Appendix, the derivation of the IHA originally given in Woltring et al. (1987) is reviewed and elaborated in more detail. Clearly, numerical implementation of the IHA algorithm requires time discretization. When discretizing the derivative $\dot{R}(t_i)$ by a one-sided difference quotient ΔR_i, the natural skew symmetry relation (A.3b) remains only approximately valid. Therefore we propose an alternative discretization procedure: When replacing pointwise evaluation $R_i = R(t_i)$ by the symmetric mean $\bar{R}_i = (R(t_{i+1}) + R(t_{i-1}))/2$ and ΔR_i by $\bar{\Delta} R_i = (R(t_{i+1}) - R(t_{i-1}))/(t_{i+1} - t_{i-1})$, the product $\bar{\Delta} R_i \cdot \bar{R}_i^T$ becomes skew symmetric again. In fact, it is straightforward to verify that

$$\begin{aligned} &(R(t_{i+1}) - R(t_{i-1}))(R(t_{i+1}) + R(t_{i-1}))^T/2 = \\ &= -((R(t_{i+1}) - R(t_{i-1}))(R(t_{i+1}) + R(t_{i-1}))^T/2)^T. \end{aligned} \tag{4}$$

Thus, the components of the rotation frequency vector $\boldsymbol{\omega}(t_i)$ are extracted from

$$\bar{\Delta} R_i \cdot \bar{R}_i^T, \tag{5a}$$

see (A.4). In a similar manner, $\boldsymbol{d}(t_i)$ is replaced such that the reference point on the axis can be extracted from

$$\bar{\boldsymbol{s}}_i = \bar{\boldsymbol{d}}_i + \frac{1}{\bar{\omega}_i^2}\left(\bar{\boldsymbol{\omega}}_i \times \bar{\Delta}\boldsymbol{d}_i\right), \tag{5b}$$

see (A.5c).

We tested both, the corrected and non-corrected IHA calculation. For exact data, the corrected approach yielded the axis direction in double precision accuracy. Fig. 1 depicts the error induced by the finite step width by relating a given flexion increment and the angle between the calculated FHA and the true axis. Furthermore, the symmetric part of $R \cdot \Delta R$ and $\bar{R} \cdot \bar{\Delta} R$ was calculated, respectively. While $R \cdot \Delta R + (R \cdot \Delta R)^T$ converges to zero with decreasing step size, $\bar{R} \cdot \bar{\Delta} R + (\bar{R} \cdot \bar{\Delta} R)^T$ is throughout in the size of rounding error. However, the discretization error has still an effect on the computed reference point $\bar{\boldsymbol{s}}(t_i)$.

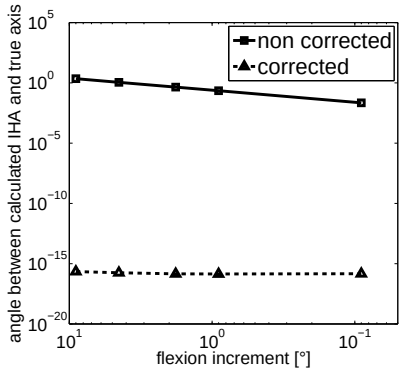

Fig. 1. IHA caclulation: Due to discretization errors depending on the angular step width the calculated axis direction deviates from the true axis direction. Squares (■) depict this effect for pure flexion data when the IHA formulas are not corrected, triangles (▲) depict the corrected version.

2.4 Data

The methods are applied to fictive data. As basis for a healthy knee joint model, the approximation as a compound hinge joint including flexion-extension and tibial rotation was taken (Asano et al. (2005); Hollister et al. (1993); Most et al. (2004); Smith et al. (2003); Eckhoff et al. (2001)). Specific data for flexion-extension and tibial rotation was taken from Moglo and Shirazi-Adl (2005).

Due to STA, skin mounted markers involve the largest error when compared with bone pins, radiography, or

MRI. STA effects may vary among individual subjects, due to the performed movement task, and due to speed or dynamics of motion. For our investigations, a perturbation typically inferred by STA is added in order to address the question which approach would be most appropriate in the presence of perturbations. Following Dumas and Cheze (2009) this STA noise is modeled via trigonometric functions. The frequency is varied for the individual markers. For simplicity, the amplitude is controlled by an overall parameter.

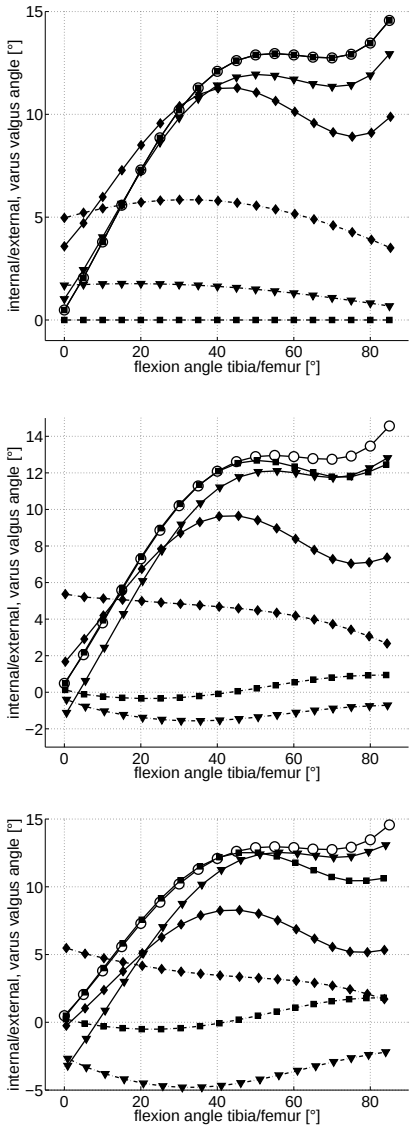

Fig. 2. Rotations represented in the JCS: Data for flexion and tibial rotation (○, Moglo and Shirazi-Adl (2005)). Displacements are computed for different flexion axes, namely, first the true axis used to generate the fictive kinematic data (■), the SARA axis (▼), and the FHA (⧫). Solid lines depict ie-rotation (tibial rotation), dash-dotted lines depict vv-rotation (adduction/abduction). The first plot shows the case without perturbation, the second one with a maximum deviation of a marker from its true position by estimated 8 mm, the third one by 15 mm.

3. RESULTS

Figs. 2 and 3 compare the computed 6 DOF joint displacements, represented in the JCS of Grood and Suntay (1983). The first axis vector, $\boldsymbol{e}_1$, of the non-orthogonal JCS is the flexion axis which is first set equal to the true axis used to generate the fictive kinematic data, then equal to the SARA axis, and finally equal to the FHA axis. The third axis, $\boldsymbol{e}_3$, of the JCS, corresponding to the tibial rotation axis, is determined from body fixed reference marker points on the tibia. The second axis, $\boldsymbol{e}_2$, also called the floating axis, is obtained as $\boldsymbol{e}_3 \times \boldsymbol{e}_1$.

Joint translations are defined as the relative movement of the tibia origin in the femur LCS, projected onto the three axes of the JCS. Fictive data was generated without joint translations. For zero noise, the joint translations for the true axis and the SARA axis are in the size of rounding error. However, the FHA axis involves finite translations due to the unavoidable discretization error in the axis' reference point. For finite noise, the 3D translations become finite in all three cases. As can be seen in Fig. 3, for larger noise the effect of the discretization error is of minor relevance and the FHA performs better than the SARA.

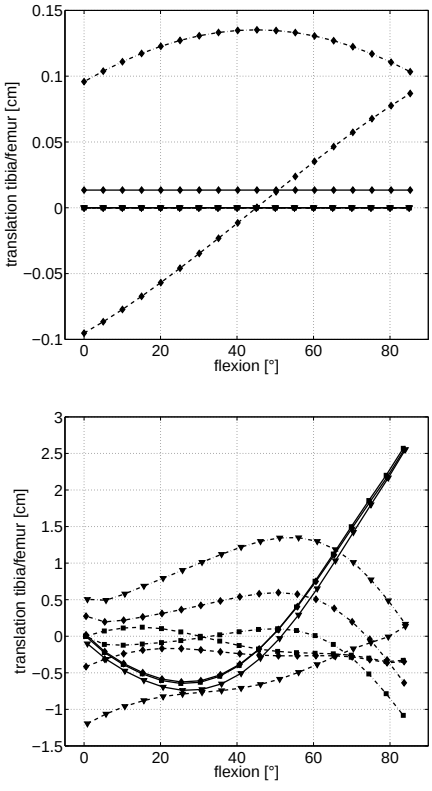

Fig. 3. Translations represented in the JCS: true axis (■), SARA axis (▼), and FHA (⧫). Solid lines depict the translation in direction of the flexion axis s_1 (medial-lateral tibial thrust), dashed lines the translation in direction of the floating axis s_2 (anterior-posterior drawer), and dash-dotted lines translation in direction of the tibial rotation axis s_3 (joint distraction-compression). The first plot is without perturbation, the second one with a maximum deviation of 15 mm.

Investigation of the joint rotations reveals significant differences between the three cases under consideration. The open circles in all plots of Figs. 2 show the true rotation profile of the fictive data. In the absence of perturbations and true reference axes the same profile can be reproduced, and the vv-rotation vanishes. The largest vv-rotation occurs for the FHA flexion axis, in the presence as well as in the absence of noise. For zero-noise and small noise, also the deviation of the internal/external (ie) rotation is largest for the FHA. For larger noise, the ie-rotation of SARA and of FHA deviate comparably from the ie-rotation obtained with the true flexion axis.

The angular deviations of the three axes are shown in Table 2. Note that even for zero noise the angle between the true flexion axis and the IHA or the SARA cannot vanish for general motion, since SARA and IHA approximate the joint as hinge or as screw axis, respectively. Coincidence of all axes occurs for rotation about a cylindrical axis only.

Table 2. Angles between reference axes.

	angle [°] between	
noise	true axis / SARA	true axis / FHA
0 mm	1.8	18.3
8 mm	1.7	19.3
15 mm	4.7	20.0

4. DISCUSSION

Apparently, the determination of the six DOF displacement by means of the FHA is more susceptible to noise. The authors speculate that the additional freedom of the FHA renders its determination less stable than the determination of the SARA axis. Note that the FHA is not obtained from a global optimization principle but by averaging local solutions in terms of the discrete IHA corresponding to pairs of time steps. Possibly, the FHA may be improved by including many combinations of time steps, at higher computational cost. In contrast, the SARA approach is based on simultaneous least squares optimization including the complete time series.

However, a trend to smaller translations s_2, s_3 is noticed for the FHA. Considering true screw motion (stable IHA), translations are only present in direction of the FHA which, playing the role of the the flexion axis, yields a translation (s_1, s_2, s_3) with $s_2 = s_3 = 0$. In the case of general motion (unstable IHA), the largest translation is s_1, whereas the other components s_2 and s_3 become small.

5. CONCLUSION

The application of different axes shows that kinematic crosstalk is non negligible, requiring a prescription for a reproducible axes calculation. The application of SARA and IHA on fictive kinematics data enables an evaluation of their performance regarding their relation to the true flexion axis.

Ultimately, clinical approvement is envisaged. Furthermore, the present investigation shows that there is some potential of improvement of the procedure by including the flexion axis and the tibial rotation axis in the the optimization (Reichl et al. (2010)).

Appendix A. DERIVATION OF THE IHA

In the local coordinate system of the body the points on the helical axis C of a rigid body are denoted by $\boldsymbol{c}_2$.[2] In the global laboratory coordinate system they transform according to

$$\boldsymbol{c}_1(t_i) = \boldsymbol{d}(t_i) + R(t_i)\boldsymbol{c}_2\,, \tag{A.1}$$

where $\boldsymbol{d}(t)$ is the vector of the origin of the local coordinate system in the global one and $R(t)$ is the instantaneous attitude matrix. With the same notation as in (1),(2), Eqn. (A.1) reads

$$\boldsymbol{c}_1(t_i) = R_1(t_i)^{-1}\big(\boldsymbol{d}_2(t_i) - \boldsymbol{d}_1(t_i) + R_2(t_i)\boldsymbol{c}_2\big)\,. \tag{A.2}$$

$R(t_i)$ can be identified with $R_1(t_i)^{-1}R_2(t_i)$ and $\boldsymbol{d}(t_i)$ with $R_1(t_i)^{-1}(\boldsymbol{d}_2(t_i) - \boldsymbol{d}_1(t_i))\,.$

The points with minimal velocity are the points of the coinciding axis for rotation and translation.

For the time derivative

$$\dot{\boldsymbol{c}}_1(t) = \dot{\boldsymbol{d}}(t) + \dot{R}(t)\boldsymbol{c}_2 + R(t)\underbrace{\dot{\boldsymbol{c}}_2}_{=0}\,,$$

relation $\boldsymbol{c}_2 = R^T(t)(\boldsymbol{c}_1(t) - \boldsymbol{d}(t))$ yields

$$\dot{\boldsymbol{c}}_1(t) = \dot{\boldsymbol{d}}(t) + \dot{R}(t)R^T(t)(\boldsymbol{c}_1(t) - \boldsymbol{d}(t))\,.$$

Differentiation of the orthogonality relation of the rotation matrix,

$$R(t)R^T(t) = R^T(t)R(t) = 1\,, \tag{A.3a}$$

$$\dot{R}(t)R^T(t) = -\big(\dot{R}(t)R^T(t)\big)^T, \tag{A.3b}$$

shows that $\dot{R}(t)R^T(t)$ is skew symmetric. Multiplication of a vector by a skew symmetric matrix can be represented by the cross product

$$\begin{pmatrix}\omega_1\\ \omega_2\\ \omega_3\end{pmatrix} \times \begin{pmatrix}x_1\\ x_2\\ x_3\end{pmatrix} = \begin{pmatrix}0 & -\omega_3 & \omega_2\\ \omega_3 & 0 & -\omega_1\\ -\omega_2 & \omega_1 & 0\end{pmatrix} \cdot \begin{pmatrix}x_1\\ x_2\\ x_3\end{pmatrix}. \tag{A.4}$$

Thus,

$$\dot{R}(t)R^T(t)\cdot(\boldsymbol{c}_1(t) - \boldsymbol{d}(t)) \equiv \boldsymbol{\omega}\times(\boldsymbol{c}_1(t) - \boldsymbol{d}(t))\,,$$

and

$$\dot{\boldsymbol{c}}_1(t) = \dot{\boldsymbol{d}}(t) + \boldsymbol{\omega}\times(\boldsymbol{c}_1(t) - \boldsymbol{d}(t))\,.$$

In the following we write $\omega := |\boldsymbol{\omega}|$.

Minimization problem: We want to find those points described by $\boldsymbol{c}_1 = \boldsymbol{c}_1(t)$ in the global system, of the rigid body with minimal velocity $|\dot{\boldsymbol{c}}_1| = \|\dot{\boldsymbol{c}}_1\|_2$. Using the identity $(\boldsymbol{a}\times\boldsymbol{b})\cdot(\boldsymbol{c}\times\boldsymbol{d}) = (\boldsymbol{a}\cdot\boldsymbol{c})(\boldsymbol{b}\cdot\boldsymbol{d}) - (\boldsymbol{a}\cdot\boldsymbol{d})(\boldsymbol{b}\cdot\boldsymbol{c})$ we see that $|\dot{\boldsymbol{c}}_1|^2$ takes the form

$$|\dot{\boldsymbol{c}}_1|^2 =$$
$$|\dot{\boldsymbol{d}}|^2 + 2\,\dot{\boldsymbol{d}}\cdot(\boldsymbol{\omega}\times(\boldsymbol{c}_1 - \boldsymbol{d})) + \omega^2\,|\boldsymbol{c}_1 - \boldsymbol{d}|^2 - (\boldsymbol{\omega}\cdot(\boldsymbol{c}_1 - \boldsymbol{d}))^2.$$

In order to minimize $|\dot{\boldsymbol{c}}_1|^2$, it is varied with respect to the points C on the body. Formally this is carried out by applying the gradient $\partial/\partial\boldsymbol{c}_1 = \nabla_{\boldsymbol{c}_1}$ to $|\dot{\boldsymbol{c}}_1|^2$. Observing the identity $\nabla_{\boldsymbol{c}_1}(\boldsymbol{a}\cdot(\boldsymbol{\omega}\times\boldsymbol{c}_1)) = \boldsymbol{a}\times\boldsymbol{\omega}$ we obtain the necessary condition for a minimum of $|\dot{\boldsymbol{c}}_1|^2$ in the form

$$\begin{aligned}0 = \tfrac{1}{2}\,\nabla_{\boldsymbol{c}_1}|\dot{\boldsymbol{c}}_1|^2 &= (\dot{\boldsymbol{d}}\times\boldsymbol{\omega}) + \omega^2\,(\boldsymbol{c}_1 - \boldsymbol{d}) + (\boldsymbol{\omega}\cdot(\boldsymbol{c}_1 - \boldsymbol{d}))\,\boldsymbol{\omega}\\ &= (\dot{\boldsymbol{d}}\times\boldsymbol{\omega}) + \omega^2\,(\boldsymbol{c}_1 - \boldsymbol{d}) + (\boldsymbol{\omega}\cdot\boldsymbol{\omega}^T)\,(\boldsymbol{c}_1 - \boldsymbol{d})\,.\end{aligned}$$

[2] The vector $\boldsymbol{c}_2$ of an arbitrary point of this object is not time dependent with respect to the local coordinate system.

The minimum condition now evaluates to

$$\boldsymbol{\omega}(t) \times \dot{\boldsymbol{d}}(t) = \underbrace{\left(\omega^2(t)\, I - \boldsymbol{\omega}(t) \cdot \boldsymbol{\omega}^T(t)\right)}_{=:\, Q(t)} \left(\boldsymbol{c}_1(t) - \boldsymbol{d}(t)\right).$$

The matrix $Q(t)$ has generic rank 2, with kernel given by $\mathrm{span}\{\boldsymbol{\omega}(t)\}$. In the exceptional case $\boldsymbol{\omega}(t) = \mathbf{0}$, $Q(t)$ is the zero matrix, and the solution of the minimization problem is not defined. For $\boldsymbol{\omega}(t) \neq \mathbf{0}$, the solution set is a line in 3D, represented by $\boldsymbol{c}_1(t) = \boldsymbol{s}(t) + \lambda\, \boldsymbol{n}(t)$, with a reference point $\boldsymbol{s}(t)$ and unit direction vector $\boldsymbol{n}(t) = \boldsymbol{\omega}(t)/\omega(t)$. A specific point $\boldsymbol{s}(t)$ can be selected as the point nearest to the origin of system two. This point has the property that its connecting line to the origin is orthogonal to the line, yielding the relation

$$\boldsymbol{\omega}^T(t) \cdot (\boldsymbol{s}(t) - \boldsymbol{d}(t)) = 0\,.$$

Then, for $\boldsymbol{c}_1(t) = \boldsymbol{s}(t)$,

$$\begin{aligned} \boldsymbol{\omega}(t) \times \dot{\boldsymbol{d}}(t) &= && \text{(A.5a)}\\ &= \omega^2(t)\,(\boldsymbol{s}(t) - \boldsymbol{d}(t)) - \boldsymbol{\omega}(t) \cdot \underbrace{\boldsymbol{\omega}^T(t) \cdot (\boldsymbol{s}(t) - \boldsymbol{d}(t))}_{=0}, \\ \boldsymbol{\omega}(t) \times \dot{\boldsymbol{d}}(t) &= \omega^2(t)(\boldsymbol{s}(t) - \boldsymbol{d}(t))\,, && \text{(A.5b)}\\ \boldsymbol{s}(t) &= \boldsymbol{d}(t) + \frac{1}{\omega(t)}\Big(\frac{\boldsymbol{\omega}(t)}{\omega(t)} \times \dot{\boldsymbol{d}}(t)\Big), && \text{(A.5c)} \end{aligned}$$

which gives the following representation for the IHA,

$$\begin{aligned} \boldsymbol{c}_1(t) &= \boldsymbol{d}(t) + \frac{1}{\omega(t)}\big(\boldsymbol{n}(t) \times \dot{\boldsymbol{d}}(t)\big) + \lambda\, \boldsymbol{n}(t)\,, && \text{(A.6a)}\\ \boldsymbol{n}(t) &= \frac{\boldsymbol{\omega}(t)}{\omega(t)}\,. && \text{(A.6b)} \end{aligned}$$

Shift speed: Rotation and translation components are orthogonal when they are described with respect to the IHA. The direction of the rotation axis is the direction of the translation. Therefore the (scalar) speed of the translation can be obtained by projecting the speed of the origin of the local system onto the unit direction vector of the IHA,

$$v(t) = \boldsymbol{n}(t) \cdot \dot{\boldsymbol{d}}(t)\,. \qquad \text{(A.7)}$$

REFERENCES

Asano, T., Akagi, M., and Nakamura, T. (2005). The functional flexion-extension axis of the knee corresponds to the surgical epicondylar axis: In vivo analysis using a biplanar image-matching technique. *The Journal of Arthroplasty*, 20(8), 1060–1067.

Camomilla, V., Cereatti, A., Vannozzi, G., and Cappozzo, A. (2006). An optimized protocol for hip joint centre determination using the functional method. *Journal of Biomechanics*, 39, 1096–1106.

Churchill, D.L., Incavo, S.J., Johnson, C.C., and Beynnon, B.D. (1998). The transepicondylar axis approximates the optimal flexion axis of the knee. *Clin Orthop*, 111–118.

Dumas, R. and Cheze, L. (2009). Soft tissue artifact compensation by linear 3d interpolation and approximation methods. *Journal of Biomechanics*, 42, 22142217.

Eckhoff, D.G., Dwyer, T.F., Bach, J.M., Spitzer, V.M., and Reinig, K.D. (2001). Three-dimensional morphology of the distal part of the femur viewed in virtual reality. *Journal of Bone and Joint Surgery American Volume*, 83-A Suppl 2 (Pt 1), 43–50.

Ehrig, R.M., Taylor, W.R., Duda, G.N., and Heller, M.O. (2006). A survey of formal methods for determining the centre of rotation of ball joints. *Journal of Biomechanics*, 39, 2798–2809.

Ehrig, R.M., Taylor, W.R., Duda, G.N., and Heller, M.O. (2007). A survey of formal methods for determining functional joint axes. *Journal of Biomechanics*, 40, 2150–2157.

Ehrig, R.M., Heller, M.O., Kratzenstein, S., Duda, G.N., Trepczynski, A., and Taylor, W.R. (2011). The score residual: A quality index to assess the accuracy of joint estimations. *Journal of Biomechanics*, 44(7), 1400–1404.

Grood, E.S. and Suntay, W.J. (1983). A joint coordinate system for the clinical description of three-dimensional motions: Application to the knee. *Journal of Biomechanical Engineering*, 105(2), 136–144.

Heller, M.O., Kratzenstein, S., Ehrig, R.M., Wassilew, G., Duda, G.N., and Taylor, W.R. (2011). The weighted optimal common shape technique improves identification of the hip joint center of rotation in vivo. *Journal of Orthopaedic Research*, 29(10), 1470–1475. doi: 10.1002/jor.21426.

Hollister, A.M., Jatana, S., Sing, A.K., Sullivan, W.W., and Lupichuk, A.G. (1993). The axes of rotation of the knee. *Clinical Orthopaedics and Related Research*, 290, 259–268.

Marin, F., Mannel, H., Claes, L., and Dürselen, L. (2003). Correction of axis misalignment in the analysis of knee rotations. *Human Movement Science*, 22, 285–296.

Martelli, S., Zaffagnini, S., Falcioni, B., and Motta, M. (2002). Comparison of three kinematic analyses of the knee: Determination of intrinsic features and applicability to intraoperative procedures. *Computer Methods in Biomechanics and Biomedical Engineering*, 5, 175–185.

Moglo, K.E. and Shirazi-Adl, A. (2005). Cruciate coupling and screw-home mechanism in passive knee joint during extensionflexion. *Journal of Biomechanics*, 38, 1075–1083.

Most, E., Axe, J., Rubash, H., and Li, G. (2004). Sensitivity of the knee joint kinematics calculation to selection of flexion axes. *Journal of Biomechanics*, 37(11), 1743–1748.

Reichl, I., Auzinger, W., Schmiedmayer, H.B., and Weinmüller, E. (2010). Reconstructing the knee joint mechanism from kinematic data. *Mathematical and Computer Modelling of Dynamical Systems*, 16, 403–415.

Schwartz, M.H. and Rozumalski, A. (2005). A new method for estimating joint parameters from motion data. *Journal of Biomechanics*, 38, 107–116.

Smith, P.N., Refshauge, K.M., and Scarvell, J.M. (2003). Development of the concepts of knee kinematics. *Arch Phys Med Rehabil*, 84, 1895–1902.

Woltring, H., de Lange, A., Kauer, J., and Huiskes, R. (1987). Instantaneous helical axis estimation via natural, cross-validated splines. In *Bergmann G, Kölbel R, Rohlmann A (eds.). Biomechanics: Basic and Applied Research. Springer*, 121–128.